Nanoscale

How soft is a single protein?: Stress-strain curve of antibody pentamers with 5 pN and 50 pm resolutions

Journal:	*Nanoscale*
Manuscript ID	NR-ART-11-2015-007957.R1
Article Type:	Paper
Date Submitted by the Author:	14-Dec-2015
Complete List of Authors:	Perrino, Alma; CSIC Garcia, Ricardo; CSIC,

How soft is a single protein?: Stress-strain curve of antibody pentamers with 5 pN and 50 pm resolutions

Alma P. Perrino and Ricardo Garcia

Instituto de Ciencia de Materiales de Madrid (CSIC),
c/ Sor Juana Ines de la Cruz 3, 28049 Madrid, Spain.

Abstract

Understanding the mechanical functionalities of complex biological systems requires the measurement of the mechanical compliance of their smallest components. Here, we develop a force microscopy method to quantify the softness of a single antibody pentamer by measuring the stress-strain curve with force and deformation resolutions, respectively, of 5 pN and 50 pm. The curve shows three distinctive regions. For ultrasmall compressive forces (5-75 pN), the protein's central region shows that the strain and stress are proportional (elastic regime). This region has an average Young modulus of 2.5 MPa. For forces between 80 and 220 pN, the stress is roughly proportional to the strain with a Young modulus of 9 MPa. Higher forces lead to irreversible deformations (plastic regime). Full elastic recovery could reach deformations amounting 40% of the protein height. The existence of two different elastic regions is explained in terms of the structure of the antibody central region. The stress-strain curve explains the capability of the antibody to sustain multiple collisions without any loss of biological functionality.

INTRODUCTION

Mechanical properties at the nanoscale have a significant role in different molecular and cell biology processes[1]. Tumor progression is favored by a remodellation of the mechanical stiffness of the extra cellular matrix[2]. Improved extensibility such as the one found in fibrin proteins is achieved via the formation of repeated units of hydrogen bonds in alpha helical folds[3]. It has been reported that the misfolding mechanisms of amyloid proteins involves fibrils of different stiffness[4]. Some proteins polymerize into spirals to accumulate elastic energy. That energy is driving force for lipid membrane deformation[5]. Secreted proteins such as pentameric IgM antibodies[6] experience multiple and unspecific collisions with other proteins, cells or extra-cellular matrix components without any loss of biological activity. This implies that protein deformation is either negligible or that the protein fully recovers its size and shape after a collision. The mechanical response of any material to a tensile or compressive load is contained in the stress-strain curve[7]. That curve has never been reported for a single and isolated protein.

Dynamic and contact atomic force microscopy (AFM) methods have been applied to measure the protein flexibility of packed arrays of proteins[8-16], and in some cases, of single proteins[17-24]. However, force microscopy methods based on the acquisition of force-curves have a major limitation to measure the stress-strain curve of a single protein. Forces and deformations are mixed in the observables. Hence, cantilever deflection is an input in both the determination of the force and the deformation. Thus the error associated with the measurement of the deflection propagest in both the force and the deformation. Neutron scattering experiments can detect the average fluctuations of the atoms in a polypeptide chain which do provide an estimation of the protein softness[25]. Optical methods in combination with gold nanoparticles have been applied to measure the viscoelastic response of some enzymes[26]. However, neutron scattering and optical

methods provide the average value of the mechanical response of an ensemble of millions of proteins.

Here we develop a dynamic force microcopy method to measure the stress-strain curve of a single protein by applying forces in the 20-300 pN range. The measurements show that a folded IgM pentamer has two elastic and one plastic region before fracture. We show that the central domain of an IgM could sustain elastic strains of about 0.4 (40% of the nominal protein thickness) which is equivalent to a compressive deformation of 2.8 nm. The elastic regime is characterized by two different elastic moduli, 2.5 MPa for very small forces (below 75 pN) and 9 MPa for applied forces between 80 and 220 pN. The ability to perform these measurements rests on several instrumental developments that enable (i) to measure, independently and simultaneously, the forces and the associated deformations (ii) the capability of imaging proteins in liquid at sub-30 pN forces.

EXPERIMENTAL METHODS

Hybrid dynamic AFM

The experiments have been performed in liquid with a Cypher S microscope (Asylum Research, Santa Barbara, USA). We have used AC-40TS cantilevers (Olympus, Japan) with typical values of $k \approx 0.07$ N/m, $f_0 \approx 25$ kHz and $Q \approx 2$ for applying forces below 120 pN. For higher forces we used OMCL-RC800PSA (Olympus, Japan) cantilevers characterized by $k \approx 0.76$ N/m, $f_0 \approx 16$ kHz and $Q \approx 2.2$. The last two parameters correspond to measurements in water. The force constant and the quality factor of the cantilevers were determined using the thermal noise method. The amplitudes used to gather the data of Figs. 2-3 were in the 1.8- 2.4 nm range. Some of the AFM images have been processed by using the WSxM program[27].

Sample preparation

Human IgM antibodies were purchased from Chemicon, Inc., USA. A 20 µl drop of $NiCl_2$ (50 mM) is deposited on a freshly cleaved mica surface and incubated for 30 seconds. $NiCl_2$ is used to functionalize the mica surface for enhancing the adsorption of the antibodies. Next a 5 μl drop taken from a 40 μg/ml of IgM antibodies diluted in PBS was injected into the $NiCl_2$ drop. After an incubation period of 60 seconds, the sample was rinsed with distilled water in order to remove weakly attached proteins.

Data analysis

The quantitative data of Figures 3(c), 3(d), 5 are the average values of 10 antibodies molecules which remained in the same conformation throughout the experiment (See Figure S3).

The deformation of the antibody as a function of the forces has been determined by comparing the height of the top of the IgM before and after the application of a force (Figure 3 and Figure S4). However, the IgM is also deformed at the smallest force applied here (22 pN). So the absolute deformation must take into account the initial deformation. The initial deformation δ_0 can be acquired from the force curve recorded on the central region of an IgM,

$$\delta_0 = \Delta z_c - z_0 \qquad (5)$$

where z_c is the piezo displacement (tip-surface separation), Δz_c is the difference in piezo displacement between the contact point z_{c1} and the piezo displacement during imaging z_{c2} (see Figure S5); z_0 is the mean deflection of the tip.

RESULTS AND DISCUSSION

The force microscopy method implemented here is a hybrid of frequency and amplitude modulation AFM methods[28-30]. From amplitude modulation AFM[31] , it incorporates the condition of keeping fixed the driving force and oscillation amplitude during imaging. From frequency modulation AFM[32] , it incorporates the condition of performing the imaging with the oscillation tuned at the actual resonant frequency. It has two main feedback loops (Fig. 1(a)). First, an image is taken while the amplitude of the oscillation is kept at fixed value. During the imaging process, the amplitude of the force that drives the oscillation of the cantilever V_{exc} is also kept at a fixed value which is higher than the one used to excite initially the cantilever $V_{exc,0}$ (≈20 nm above the antibodies). The second loop tracks the actual resonant frequency of the microcantilever so the oscillation is always phase shifted 90º degrees with respect to the driving force. The first feedback loop provides a robust imaging process and enables the acquisition of high resolution images at very small forces. The second loop enables the accurate determination of the force (more details in SI). The use of a *z*-feedback loop based on keeping constant the driving voltage while imaging has been proposed as an alternative to frequency modulation AFM operation in air or liquid[32-34]. There the changes in the nature of the force (attractive versus repulsive) could destabilize the frequency feedback loop of the microscope.

Measuring the mechanical response of a single protein near physiological conditions is challenging for at least two reasons, (i) the small value of the forces involved in generating elastic deformations and (ii) the need to combine force measurements with high resolution images of single proteins. As the experimental sample, we chose pentameric antibodies (IgM)

(see SI). This is the first type of antibody that enters the bloodstream upon infection. It has five identical monomers, each of them made of two fragment antigen binding regions Fab and a tail fragment Fc[35] (Fig. 1(b)). It also contains a J-chain that links two contiguous Fc fragments. The IgM offers a distinctive morphology that allows its unambiguous identification by force microscopy. The adhesion force between the mica substrate and the IgM in liquid is very small. During the measurements is not uncommon to see the protein displaced by the lateral force of the tip. This fact also emphasizes the relevance of applying sub-50 pN forces while imaging proteins. The experimental method involves the application of several forces on a single protein and the measurement of the resulting deformations. The last aspect requires the acquisition of high resolution images with lateral and vertical values, respectively, of 2 nm and 0.05 nm. We note that with a single microcantilever we could not cover the range of forces applied here (20 to 300 pN). For that reason very soft cantilevers (~0.07 N/m) have been used to apply forces in the 20 to 120 pN range while stiffer cantilevers (~ 0.7 N/m) have been used to apply forces in the 100 to 300 pN range. There is a force region around 100 pN were both cantilevers could be used to perform the measurements. This overlap will enable to record the stress-strain curve without discontinuities.

By measuring the height difference of the protein before, during and after the application of a given force we determine the protein's deformation and its nature, elastic or plastic. A force causing a plastic deformation will produce a permanent reduction of the maximum protein height. By separating the elastic and plastic regimes we determine the Young modulus and yield strength of the protein. To simplify the analysis, the height measurements are taken on the protein central region. This region is easily identified. It is also independent of any change of the molecule orientation with respect to the mica surface.

Figure 2 shows several high resolution AFM images of IgM antibodies deposited on mica. The measurements are performed with the proteins and the microcantilever-tip ensemble immersed in water at 30ºC. The random deposition process and the flexibility of the proteins generates several morphologies, notably some molecules show a pentameric structure (Fig. 2(a)). The high resolution images show a central region surrounded by five protrusions with an overall pentameric structure (Fig. 2(b) and 2(c)). The central region has a diameter of about 15 nm while its maximum height is force dependent (Fig. 3(a)-(c)). The images are in agreement with the structure deduced from homology considerations and cryo-microscopy measurements[35]. They also agree with previous AFM measurements[21]. Under a force of 22 pN we estimate an initial elastic deformation of the central region of 1.1 nm (see Methods). The above images represent raw data without corrections from the tip-protein convolution effects.

The experiment to determine the stress-strain curve of a single IgM protein is divided in two steps. First we perform measurements in the elastic regime by applying very small forces (sub-80 pN range). Figure 3(a) shows the cross-section of the central region of the IgM as a function of the applied force. The force applied on the protein is determined by using Sader-Jarvis' method[36] (see SI for the expression). In this experimental run, we have applied six forces of 22, 30, 37, 47, 65 and 22 pN. To facilitate the comparison we plot the height cross-sections at F_1, F_5 and F_6 (Fig. 3(b)). The top height at F_1 and F_6 do coincide. This observation underlines the elastic character of the deformations. We note that by increasing the force from 22 pN to 65 pN the maximum height of the central region decreases by 0.9 nm (Fig. 3(c)). Similar results have been obtained with other IgM molecules (See SI, Fig. S4). We also observe that the small peak associated to a Fab fragment that has disappeared in the profile taken at 65 pN is recovered once the force is lowered to 22 pN. The lateral component of the force during imaging induces some

rotation in the IgM; this could explain the shape mismatches observed at the protein sides. The uncertainty in the force increases with the applied force. This is due to the dependence of the force reconstruction algorithm on the observables (see SI).

There are several methods to determine the effective Young modulus E_{eff} of a material[25,37] from AFM measurements. The dominant approach is by fitting the force versus deformation data with a contact mechanics model. The use of continuum elastic models to describe the deformation of biomolecules is supported by molecular dynamics simulations[38]. We have applied this method to the central region of the IgM by using the model proposed by Chadwick and co-workers. This model removes the effect of the substrate stiffness on the measurement[39-40]. The bottom effect Hertz correction (BEHC)[39] model expresses the force as

$$F_{BEHC} = F_{Hertz}\left[1 + 1.773\frac{\sqrt{R\delta}}{h} + 1.71\frac{R\delta}{h^2} + 1.022\frac{(R\delta)^{3/2}}{h^3} + 0.13\frac{(R\delta)^4}{h^4}\right] \quad (1)$$

with

$$F_{Hertz} = \frac{4}{3}E_{eff}\sqrt{R}\delta^{3/2} \quad (2)$$

where R is the probe radius, h the protein thickness (height) and δ the deformation. To deduce the coefficients of Eq. 1, we have assumed a Poisson's ratio for the protein of 0.3. In the following calculation we have used R= 8 nm. This value has been deduced by comparing the size and shape of the high resolution images of the IgM (Fig. 2(b)-(c)) with the size and shape obtained by computing simulations using a probe of that radii[41]. In general, proteins are several orders of magnitude more compliant than a silicon tip, then the effective Young modulus of the probe-protein interface E_{eff} coincides with the one of the protein ($E_{eff} \approx E$(protein)).

By fitting the data to the contact mechanics models (Fig. 3(d)) we deduce an effective Young modulus of 2.5 MPa for BEHC. The above values are in the same order of magnitude range that the ones deduced by computer simulations of the AFM dynamics[42]. The data corresponds to the central region of IgM pentamer (Fc domains and J-chain). We also plot the data obtained with Hertz contact mechanics for completeness (4.9 MPa). Hertz contact mechanics gives higher values because is based on a semi-infinite solid. This assumption might not be satisfied when characterizing very thin specimens such as an IgM protein (~7 nm).

To determine the complete stress-strain curve of IgM requires to apply forces that produce plastic deformations. By using a stiffer cantilever (~0.7 N/m) we were able to apply forces of a few hundreds of pN (Fig. 4). The experiments show an IgM that has been imaged at 230 pN then at 315 pN and finally at 230 pN. The three height profiles do not coincide which indicates a plastic deformation. This is in contrast what was obtained by applying smaller forces (Fig. 3(b)).

To transform the data of Figures 3 and 4 into a stress-strain curve we have calculated a mean compressive stress over the protein central region by

$$\sigma = \frac{F}{\pi a^2} = \frac{F}{\pi R \delta} \qquad (3)$$

where F is the applied force and a the contact radius. The yield strength could be determined from the above equation by measuring the smallest force F_m that generates a permanent deformation of the central region of the antibody, this also will determine the yield point[43].

By introducing the elastic and plastic deformation data into equation 3 we generate the stress-strain curve of the central region of the antibody (Fig. 5(a)). The curve shows the elastic and plastic regimes. In particular, the elastic region is divided in two sections. First, the stress

increases linearly with the strain (0.15 to 0.3 range). We propose that the mechanical response in this region is dominated by the elastic deformation of Cμ4 domains (mostly beta-sheets). At higher strains (0.3-0.4) there is significant increase in the slope. This could indicate the participation of Cμ3 domains. Those domains lie below the Cμ4 domains in the mushroom shaped IgM structure[35] (Fig. 1(b)). The shaded region (strains below 0.15) has not been measured. To access that region requires the application of forces in the sub-10 pN range. Room temperature operation of an AFM (imaging mode) at those forces is beyond the state-of-the-art.

The shape of the above stress-strain curve has similarities with some curves measured on macroscopic polycrystalline materials such as iron alloys[7]. This observation underlines a common property in mechanical deformation that spans different length scales and crystalline structures. However, the maximum stress of a single protein before plastic deformation is about two orders of magnitude smaller than the one of a metal. In addition, the central region of the IgM is about 10^2 times more deformable than some iron alloys. On the other hand, the stress-strain curve reported here shows similarities as well as differences with respect to the curves obtained from macroscopic measurements performed on elastic proteins[44-46].

In the elastic regime, the Young modulus is the proportional factor between the stress σ and the strain ε.

$$\sigma = E\varepsilon \qquad (4)$$

From the stress-strain curve we obtain slopes of 5 MPa and 17 MPa for the first and second elastic regions. However those numbers should take into account the influence of the rigid mica substrate on the measurements. After the correction we obtain 2.5 and 9 MPa. We note that at low strains the Young modulus derived from the stress-strain curve and the one deduced from

the force curve (Fig. 3(d)) are identical. This agreement demonstrates the validity of the hybrid dynamic AFM method to determine the stress-strain curve.

The central region (Fc fragments and J-chain) can sustain elastic strains of 0.4 (about 40% of the nominal protein height, 7.1 nm). Those values explain the capability of IgM antibodies to sustain multiple collisions with other proteins, cells and tissues without any loss of biological functionality. The maximum contact stress for thermal induced collisions is estimated to be in the 0.1-0.5 pN/nm^2 range, this is, a few times smaller than the yield strength of the IgM. The yield strength of the protein also places a limit to the value of the forces used for high resolution and non-invasive imaging of biomolecules[47-55]. Those forces are protein dependent. However, for globular-like proteins with a secondary structure dominated by beta-sheets, we expect a similar trend, consequently forces above 200 pN should not be applied during AFM imaging.

The value of the effective Young modulus could also influence the early stages of the antibody-antigen recognition process. We suggest that an E_{IgM}~2.5 MPa maximizes the non-specific work of adhesion while enabling the protein lateral diffusion by random-walk processes[55]. Our analysis is based on the relationship between deformation and work of adhesion, $W_{adh} \propto \gamma\delta r_p \propto \gamma(r_p/E_{eff})^{2/3}$, where γ and r_p are, respectively, the surface energy of the bacterial surface-IgM interface and the effective radius of central region of the protein. The E of IgM optimizes the non-specific adhesion with respect to the values of very compliant (1-10 kPa, such as cells) and rather stiff (1 GPa, such as a virus) biomolecules. The relative work of adhesion (all the other parameters constant) scales as W_{adh}(5 MPa)/W_{adh}(10 kPa) =0.016 and W_{adh}(5 MPa)/W_{adh}(1 GPa) =34. A very compliant response will hinder the lateral diffusion while a stiffer response will imply a negligible work of adhesion. The protein will have a high probability of being released from the surface after a collision.

CONCLUSIONS

We have developed a force microscopy method to quantify the softness of a single antibody pentamer by measuring the stress-strain curve. The method enables to control the application of 20 pN forces in liquid and at room temperature with force and deformation resolutions, respectively, of 5 pN and 50 pm. The stress-strain curve shows three distinctive regions. For low strains the protein's central region shows that the stress and strain are proportional (elastic regime). This region has an average Young modulus of 2.5 MPa. For strains between 0.25 and 0.4, the data suggests a different elastic region where the stress is roughly proportional the strain with a Young modulus of 9 MPa. Higher strains lead to generation of irreversible deformations (plastic regime). The existence of two different elastic regions is explained in terms of the complex structure of the antibody central region. The Young modulus of the central region of protein measured from force curves and contact mechanics models coincides with the one deduced from the stress-strain curve. This agreement validates the hybrid dynamic AFM method to determine the stress-strain curve of proteins. The deformability of the antibody explains its capability to sustain multiple collisions without any loss of biological functionality.

ACKNOWLEDGMENT

We thank helpful discussions with J.C. Alonso (CNB, CSIC). This work was supported by grants from MINECO (Spain), CSD2010-00024 and the European Research Council ERC-AdG-340177 (3DNanoMech).

REFERENCES AND NOTES

1. P. Egan, R. Sinko, P.R. LeDuc and S. Keten, *Nat. Commun.* 2015, **6,** 7418.

2. J. G. Goetz, S. Minguet, I. Navarro-Lérida, J. J. Lazcano, R. Samaniego, E. Calvo, M. Tello, T. Osteso-Ibañez, T. Pellinen, A. Echarri, A. Cerezo, A. J. P. Klein-Szanto, R. Garcia, P. J. Keely, P. Sanchez-Mateos, E. Cukierman and M. A. Del Pozo, *Cell* 2011, **146,** 148-163.

3. A. A. Gautieri, S. Vesenteni, A. Redalli and M. J. Buehler, *Proc. Natl Acad. Sci.* 2007, **104,** 16410.

4. S. Zhang, M. Andreasen, J. T. Nielsen, L. Liu, E. H. Nielsen, J. Song, G. Ji, F. Sun, T. Skrydstrup, F. Besenbacher, N. C. Nielsen, D. E. Otzen and M. Dong, *Proc. Nat. Acad. Sci.* 2013, **110,** 2798-2803.

5. N. Chiaruttini, L. Redondo-Morata, F. Humbert, M. Lenz, S. Scheuring and A. Roux, *Cell* 2015, In Press.

6. W. E. Paul, *Fundamental Immunology*, Lippincott Williams & Wilkins, Philadelphia, 2003, Ch. 4.

7. H. F. Boyer, *Atlas of stress-strain curves,* ASM International, 2002.

8. M.D. Dong and O. Sahin, *Nature Nanotech.* 2009, **4,** 514-517.

9. J. Lu, J. Yang, M. Dong and O. Sahin, *Nanoscale* 2014, **6,** 7604-7608.

10. S. Zhang, H. Aslan, F. Besembacher and M.D. Dong, *Chem. Soc. Rev.* 2014, **43,** 7412-7429.

11. I.D. Medalsy and D.J. Muller, *ACS Nano.* 2013, **7,** 2642-2650.

12. Y. F. Dufrene, D. Martinez-Martin, I. Medalsy, D. Alsteens and D. J. Muller, *Nat. Methods* 2013, **10,** 847-854.

13. F. Rico, C.M. Su and S. Scheuring , *Nano Lett.* 2011, **11,** 3983-3986

14. J. Preiner, A. Horner, A. Karner, N. Ollinger, C. Siligan, P. Pohl and P. Hinterdorfer, *Nano Lett.* 2015, **15,** 759-763

15. K. Voitchovsky, S. A. Contera, M. Kamihira, A. Watts and J.F. Ryan, *Biophys. J.* 2006, **90,** 2075-2085.

16. E. T. Herruzo, H. Asakawa, T. Fukuma and R. Garcia, *Nanoscale.* 2013, **5,** 2678-2685.

17. R. Afrin, M.T. Alam and A. Ikai, *Protein Sci.* 2005, **14,** 1447-1457.

18. A. Ikai, R. Afrin and H. Sekiguchi, *Curr. Nanosci.* 2007, **3,** 17-29.

19. A. Ikai, *The World of Nano-Biomechanics*. Elsevier B.V. Amsterdam, The Netherlands, 2008; pp. 148-154

20. D. Martinez-Martin, E.T. Herruzo, C. Dietz, J. Gomez-Herrero and R. Garcia, *Phys. Rev. Lett.* 2011, **106,** 198101.

21. R. Garcia, E. T. Herruzo, *Nat. Nanotechnol.* 2012, **7,** 217-226.

22. M. Pfreundschuh, D. Altsteens, M. Hilbert, M.O. Steinbmetz and D.J. Muller, *Nano Lett.* 2014, **14,** 2957-2964.

23. A. Voss, C. Dietz, A. Stocker and R.W. Stark, *Nano Res.* 2015, **8,** 1987-1996

24. M. Chyasnavichyus, S. L. Young, V. V. Tsukruk, *Jpn. J. Appl. Phys.* 2015, **54,** 08LA02.

25. G. Zaccai, *Science.* 2000, **288,** 1604-1607.

26. A. Ariyaratne, C. H. Wu, C. Y. Tseng and G. Zocchi, *Phys. Rev. Lett.* 2014, **113,** 198101.

27. I. Horcas, R. Fernandez, J. M. Gomez-Rodriguez, J. Colchero, J. Gomez-Herrero, A. M. Baro, *Rev. Sci. Instrum.* 2007, **78,** 0130705.

28. G. Binnig, C. F. Quate and C. Gerber, Phys. Rev. Lett., 1986, **56,** 930.

29. C. Loppacher, R, Bennewitz, O. Pfeiffer, M. Guggisberg, S. Schär, V. Barwich, A. Baratoff and E. Meyer, *Phys. Rev. B.* 2000, **62,** 13674.

30. R. Garcia and R. Perez, *Surf. Sci. Rep.* 2002, **47,** 197.

31. R. Garcia and A. San Paulo, *Phys. Rev. B.* 1999, **60,** 4961.

32. T. R. Albretch, P. Grütter, D. Horne and D. Rugar, *J. Appl. Phys.* 1991, **69,** 668.

33. S. P. Jarvis, H. Tokumoto, H. Yamada, K. Kobayashi, and A. Toda, *Appl. Phys. Lett.* 1999, **75,** 3883-3885.

34. J. I. Kilpatrick, A. Gannepalli, J. P. Cleveland and A. P. Jarvis, *Rev. Sci. Instrum.* 2009, **80,** 023701.

35. M. Jaafar, D. Martínez-Martín, M. Cuenca, J. Melcher. A. Raman and J. Gómez-Herrero, *Beilstein J. Nanotechnol.* 2012, **3,** 336-344.

36. D. M. Czajkowsky and Z. Shao, *Proc. Natl. Acad. Sci. USA*. 2009, **106,** 14960.

37. J. E. Sader and S. P. Jarvis, *Appl. Phys. Lett.* 2004, **84,** 1801-1803 .

38. E. T. Herruzo, A. P. Perrino and R. Garcia, *Nature Commun.* 2014, **5,** 3126-3204.

39. W. H. Roos, M. M. Gibbons, A. Arkhipov, C. Uetrecht, N. R. Watts, P. T. Wingfield, A. C. Steven, A. J. R. Heck, K. Schulten, W. S. Klug, G. J. L. Wuite, *Biophys. J.* 2010, **99,** 1175-1181.

40. E. K. Dimitriadis, F. Horkay, J. Maresca, B. Kachar and R. S. Chadwick, *Biophys. J.* 2002, **82,** 2798-2810.

41. N. Gavara and R. S. Chadwick, *Nature Nanotech.* 2012, **7,** 733-736.

42. N. R. Voss and M. Gerstein, *Nucleic Acids Res.* 2010, **38,** W555-W562.

43. H. V. Guzman, P.D. Garcia and R. Garcia, *Beilstein J. Nanotechnol.* 2015, **6,** 369-379.

44. V. Vahdat and R. W. Carpick, *ACS Nano.* 2013, **7,** 9836-9850.

45. J. Gosline, M. Lillie, E. Carrington, P. Guerette, C. Ortlepp, and K. Savage, *Phil. Trans. R. Soc. London B.* 2002, **357,** 121-132.

46. A. A. Gautieri, S. Vesenteni, A. Redalli and M. J. Buehler, *Nano Lett.* 2011, **11,** 757-766.

47. L. F. Deravi, T. Su, J. A. Paten, J. W. Ruberti, K. Bertoldi and K. K. Parker, *Nano Lett.* 2012, **12,** 5587-5592.

48. D. J. Muller, F. A. Schabert, G. Buldt and A. Engel, *Biophys. J.* 1995, **68,** 1681-1686.

49. J. X. Mou, S. T. Sheng, R. Y. Ho and Z. Shao, *Biophys. J.* 1996, **71,** 2213-2221.

50. A. San Paulo and R. Garcia, *Biophys. J.* 2000, **78,** 1599-1605.

51. S. Ido, H. Kimiya, K. Kobayashi, H. Kominami, K. Matsushige and H. Yamada, *Nat Mater.* 2014, **13,** 264-270.

52. S. Ido, K. Kimura, N. Oyabu, K. Kobayashi, M. Tsukada, K. Matsushige and H. Yamada, *ACS Nano.* 2013, **7,** 1817-1822.

53. T. Uchihashi, R. Lino, T. Ando and H. Noji, *Science*. 2011, **333,** 755-758.

54. H. Asakawa, K. Ikegami, M. Setou, N. Watanabe, M. Tsukada and T. Fukuma, *Biophys. J.* 2011, **101,** 1270-1276.

55. D. Kim and O. Sahin, *Nature Nanotech* .2015, **10,** 264-269.

56. I. Casuso, J. Khao, M. Chami, P. Paul-Guilloteaux, M. Husain, J. Duneau, H. Stahlberg, J. Sturgis and S. Scheuring, *Nature Nanotech*. 2012, **7,** 525-529.

FIGURES

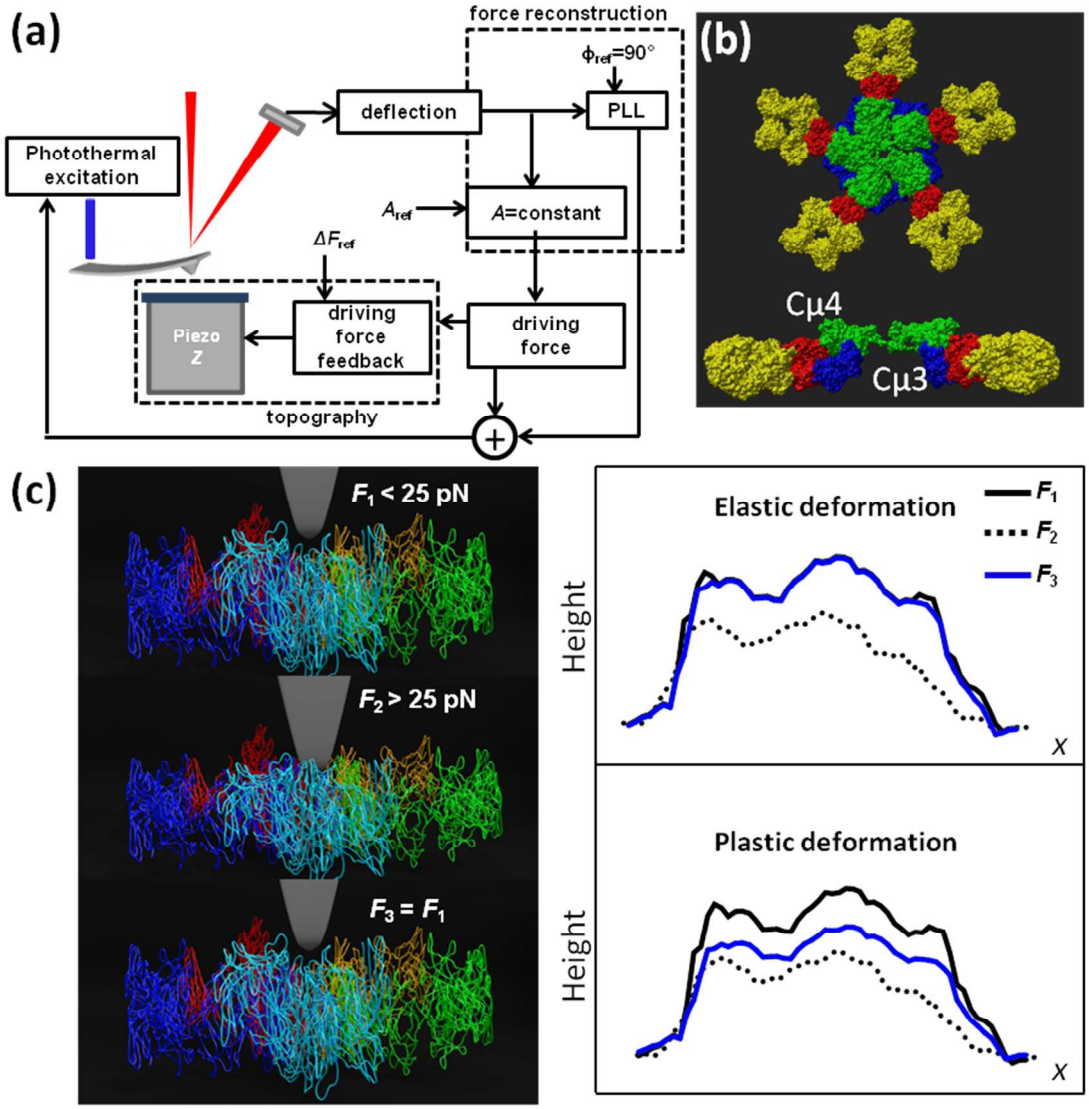

Figure 1. Scheme of the experimental setup and the force microscopy method. (a) Scheme of the hybrid dynamic force microscopy method. The relationship between the main feedback loops and the associated physical processes. (b) IgM pentamer model. The bottom figure shows a cross-section (only two monomers are shown). The Cμ4 and Cμ3 domains are marked. Fab domains are colored in yellow and the central region formed by the association of the Fc tails of the monomers is shown in green[35]. (c) Scheme of the method to measure the stress-strain curve of a single antibody. The undistorted profile of a single protein is recorded at a very small force (~25 pN), afterwards the protein profile is recorded at higher forces. Forces producing non-permanent changes in the height profile enable the determination of the protein's elastic parameters while the onset of permanent deformations marks the transition to the plastic regime.

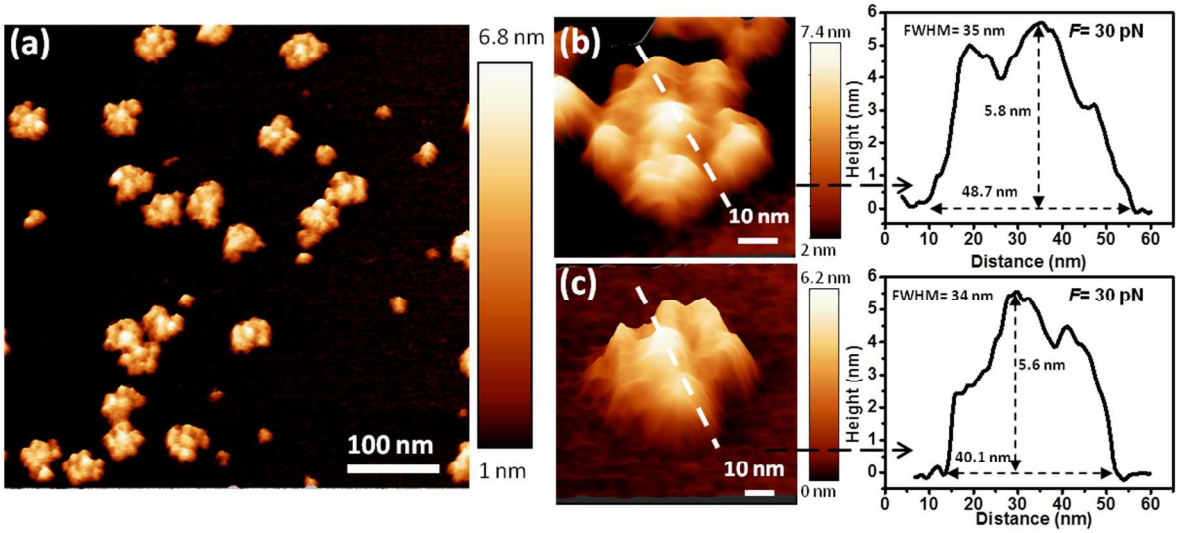

Figure 2. High resolution (height representation) AFM images of IgM antibodies in liquid. (a) IgM antibodies deposited on a mica surface. Several individual IgM pentamers are imaged. (b) High resolution AFM image of a single IgM and cross-section along the dashed line. The pentameric structure is fully resolved. (c) High resolution AFM image of a single IgM and cross-section along the dashed line. Full width at half height maximum is provided.

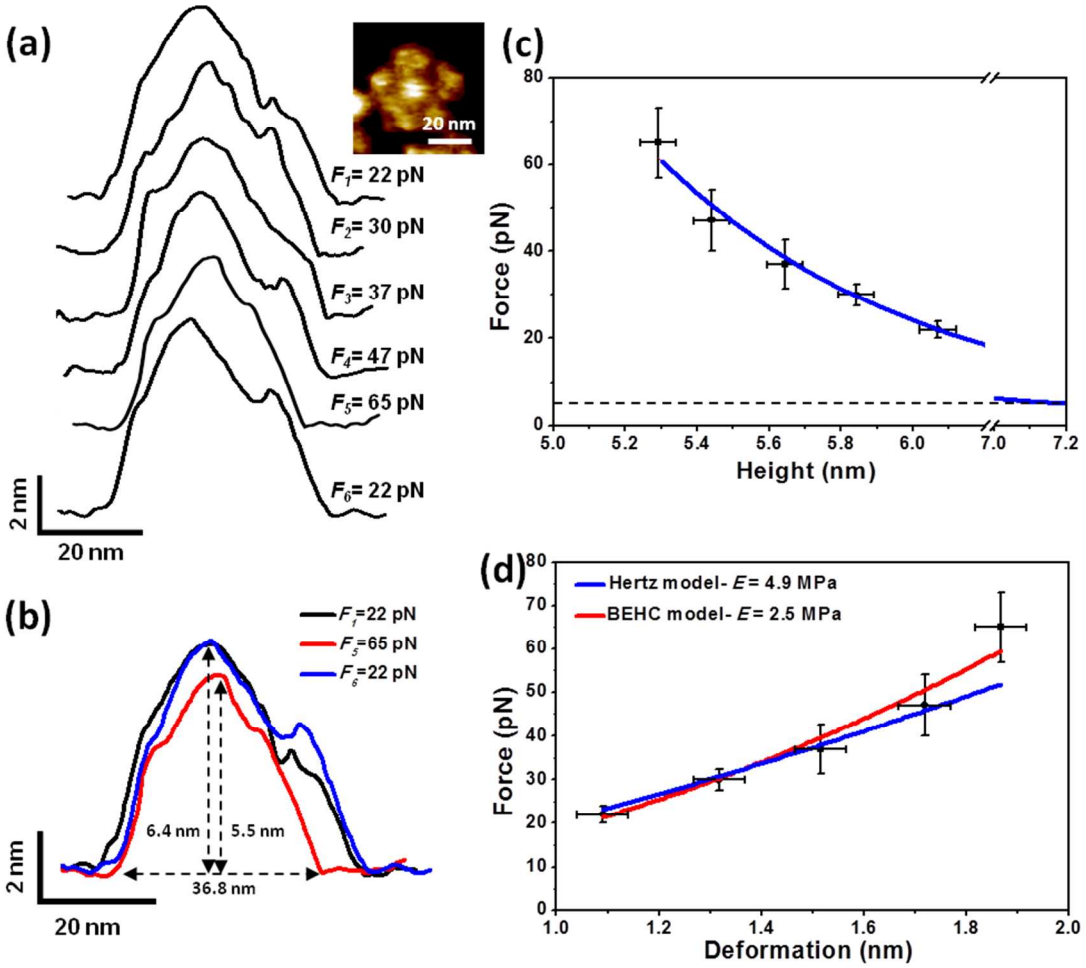

Figure 3. Forces and non-permanent deformations on single IgM antibodies in liquid. (a) Deformation of a single IgM under different forces. The experimental run involves the application of six different forces and the measurement of the resulting deformations in the sequential order of 22, 30, 37, 47, 65 and 22 pN. The height profiles have been vertically displaced for clarity. The inset shows an AFM image of the IgM. (b) Comparison of the height profiles for 22 pN (initial), 65 pN (maximum force in this experimental run) and 22 pN (final). (c) Experimental relationship between the applied force and the height of the top of an IgM. By extrapolating the data we deduce that a force of 5 pN will be needed to measure the IgM with a negligible deformation (~0.1 nm). (d) Plot of the force versus the deformation in the elastic regime. The data is fitted to BEHC and Hertz contact mechanics models.

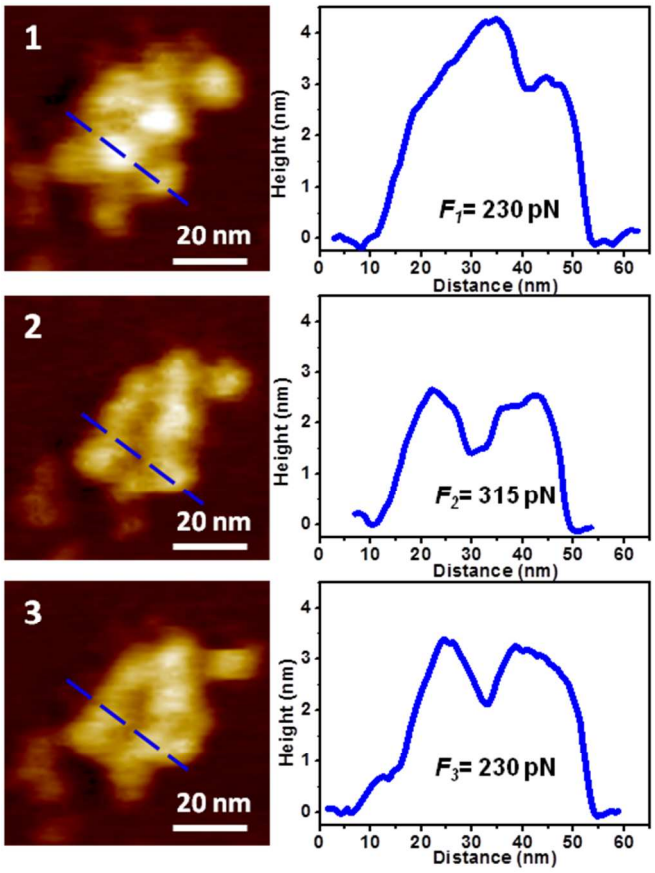

Figure 4. Protein plastic deformation**.** Images and height profiles of a single IgM before and after the onset of plastic deformation. The right panel shows the profile across the marked line in left panel. The forces applied during imaging are indicated.

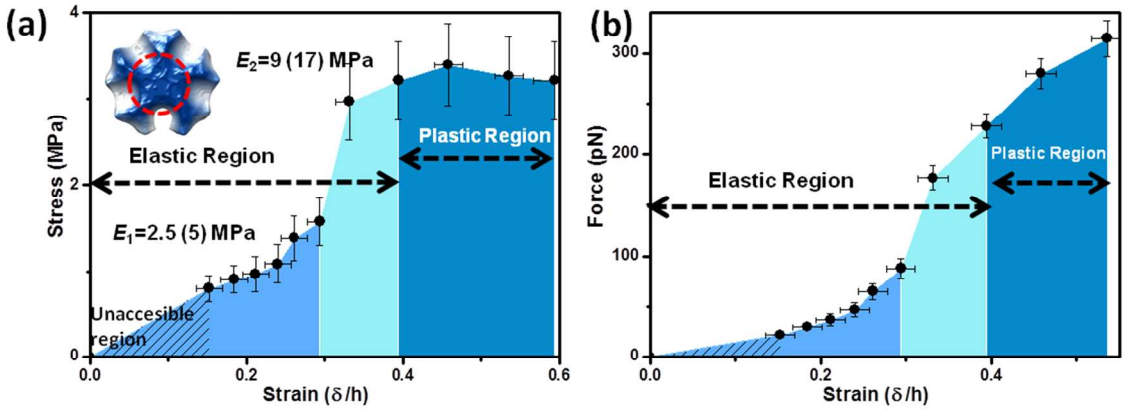

Figure 5. (a) Stress-strain curve of a pentameric IgM in liquid. The elastic, plastic and yield point are marked. The measurements are performed on the central region of the antibody (inset, ~15 nm in diameter). This region is formed by five Fc domains and the J-chain. The Young modulus values have been corrected from the influence of the substrate. The values obtained directly from the slope of stress-strain curve are indicated in parenthesis. (b) Forces applied to determine the stress-strain curve. The shaded region involves the application of forces beyond the state-of-the art of AFM.